NUMERICAL SIMULATION AND *IN VITRO* EXPERIMENTAL TESTING OF A HGMS FILTER FOR EXTRACORPOREAL BLOOD PURIFICATION

V. BĂDESCU*, LAURA ELENA UDREA*, O. ROTARIU*, RODICA BĂDESCU**, GABRIELA APREOTESEI**

*National Institute of Research and Development for Technical Physics, 47 Mangeron Blvd., Iaşi, Romania, e-mail: bav08@phys-iasi.ro
**Department of Physics, "Gh. Asachi" Technical University, 67 Mangeron Blvd, Iaşi, Romania

Abstract. Our work presents some results of numerical simulations and *in vitro* testing of a magnetic filtration system designed for removing toxin-bounded magnetic microspheres previously administered intravenously in the bloodstream of human body. The filter consists of an array of biocompatible capillary tubing and magnetizable wires adjacent in the exterior of these (axial HGMS cells). The wires are magnetized perpendicular to their axes by a spatially uniform magnetic field. First, the capture efficiency of a single filtration cell was analyzed using a mathematical model. Second, the one-pass effectiveness to remove magnetic chitosan microspheres from solutions simulating human blood was experimentally verified. Based on mathematical modelling which relates the separation cell geometrical and operational parameters, we present a criterion for the optimization of the recovery, for which the theoretical filtration efficiency is 100%. The theoretical and experimental data correlated well at low flow velocities (< 4.5 cm/s) and high magnetic fields (> 48 kA/m). Our model filter unit removed > 90% in a single pass of the magnetic microspheres (1–3 μm diameter and 450 kA/m saturation magnetization) from water at mean flow velocity ≤ 8.0 cm/s and from blood mimic fluids (ethylene glycol – water solutions) at mean flow velocity ≤ 2.0 cm/s.

Key words: magnetic particles, filter, extracorporeal, blood purification.

INTRODUCTION

Our work focuses on developing a system based on superparamagnetic carrier nanospheres for selective and rapid decorporation of biological, chemical and radioactive biohazards from humans. Current clinically important and relevant detoxification methods include haemodialysis and haemofiltration, plasmapheresis, extracorporeal immuno-absorption and direct injection of chelators and antibodies. Although these technologies are critical for the treatment of specific disease entities, the majority of biohazard exposures, medication intoxications and self-generated (auto-immune) toxins cannot be adequately treated or removed from the human body. Hence, current treatment approaches for human detoxification, not

only restrict the effectiveness, repeatability and in-field use of any of these techniques, but they are also unable to specifically and selectively target within and actively remove blood-borne toxins from the circulation. Therefore, an improvement of contemporary detoxification methods is needed.

Recently, a more active approach utilizing magnetic carriers and magnetic separation [2, 5, 6] was proposed. The system utilizes superparamagnetic composite nanospheres, that are injected directly into the blood stream of biohazard exposed humans. Receptors are attached to the surfaces or encapsulated within the polymer nanospheres, depending on the application. Once injected, the spheres circulate freely through the blood stream, selectively capturing blood-borne toxins to the specific receptors. After an appropriate time interval, the toxin-bearing nanospheres are removed from the human blood stream using an extracorporeal, closed-loop tubing system attached to a compact magnetic filter device, the detoxified blood being returned into the body.

In this context, we conceived a high gradient magnetic separator (HGMS) device suitable for biomedical applications [1, 4]. Conceptually, the magnetic separator in the system utilizes a dual-lumen needle for arterial or venous access through the skin to provide an extracorporeal blood flow through a short segment of catheter tubing. The blood leaving the body flows through the catheter tube and into an array of axial HGMS cells, consisting of biocompatible capillary tubing and magnetizable wires adjacent in the exterior of these. The entire array of tubes and wires is positioned between two permanent magnets. The net result is a magnetic force that causes the magnetic nano/micro-spheres to be deflected towards the wires and collected on the walls of the tubes. The magnetically filtered blood then flows out of this array, through another section of catheter tubing, and then through the dual-lumen needle, and back into the body.

Our first goal is to establish an optimized, basic functional cell of the separator device which allows high separation efficiency. By analyzing the trajectories of individual particles inside the clean tube of a separator cell, the capture length and the isotelic curves are established. Considering these, the capture cross-section and the conditions of maximum particle recovery are determined. The second objective of this study was to investigate the *ex vivo* removal of magnetic nano/micro-spheres from viscous fluids (water and ethylene glycol – water solution) using one cell of the magnetic separator.

MATHEMATICAL MODELLING

We analyzed the trajectory of a particle in the system presented in Figure 1. The cylindrical ferromagnetic wire of radius a, length L and saturation magnetization M_s is fixed along the Oz axis and magnetized to saturation by a

magnetic field with the intensity H_0, applied along the Ox axis. The cylindrical tube, with inner radius R and length L, is fixed along O'z' axis, coplanar with the Oz axis in the plane $y = 0$, at a distance d.

A spherical superparamagnetic particle with radius b and magnetic susceptibility χ_p is carried by a liquid with magnetic susceptibility χ_f. We consider the particle small enough to neglect its weight and inertia.
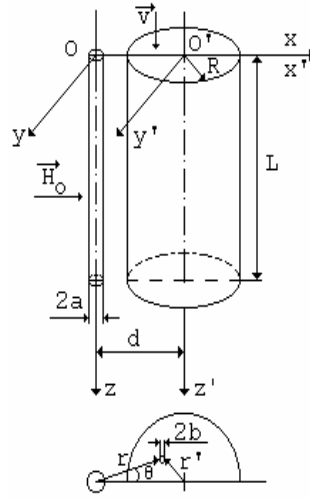
Fig. 1. Schematic diagram of the analyzed system.

The equations of particle motion under the action of magnetic and hydrodynamic drag forces are:

$$\frac{d r_a}{d t} = -\frac{v_m}{a}\left(\frac{K}{r_a^5} + \frac{\cos 2\theta}{r_a^3}\right), \tag{1a}$$

$$r_a \frac{d\theta}{d t} = -\frac{v_m}{a}\frac{\sin 2\theta}{r_a^3}, \tag{1b}$$

$$\frac{d z_a}{d t} = \frac{\bar{v}}{a}\frac{2}{R_a^2}\left(R_a^2 - r_a^2 - d_a^2 + 2 r_a d_a \cos\theta\right), \tag{1c}$$

where v_m ($= 2\mu_0 \chi M_s H_0 b^2 / 9\eta a$) is the "magnetic velocity" [3, 7], a coefficient with the dimensions of a velocity (having also the significance of the particle terminal velocity in the (r, θ) plane under the concurrent influence of the magnetic

and drag forces at $r_a = 1$ and $\theta = 0$), $\bar{v}$ is the velocity averaged across the tube section for a completely established laminar flow, $\chi = \chi_p - \chi_f$ and μ_0 is the magnetic permeability of the void space, $K = M_s / 2H_0$ for $H_0 \geq M_s / 2$ and $K = 1$ for $H_0 < M_s / 2$. The subscript *a* denotes that the corresponding parameters will be reported to the radius of the ferromagnetic wire if it represents a length.

By eliminating the time in Eqs. (1a) and (1b), one obtains an equation

$$\frac{\mathrm{d}\, r_a}{\mathrm{d}\, \theta} = \frac{K}{r_a \sin 2\theta} + r_a \operatorname{ctg} 2\theta, \tag{2}$$

whose solution represents the equation of trajectory in the (r, θ) plane:

$$r_a^2 = C \sin 2 \left(\theta - \alpha \right). \tag{3}$$

In Eq. (3), *C* and α are two constants depending on r_{a0} and θ_0, the initial values of r_a and θ. Except for the case when $\sin 2\theta_0 = 0$, which, in the analyzed system, corresponds to $\theta_0 = 0$, they have expressions:

$$C = \frac{\left(r_{a_0}^4 + 2K^2 r_{a_0}^2 \cos 2\theta_0 + K \right)^{1/2}}{\sin 2\theta_0}, \quad \alpha = \frac{1}{2} \operatorname{arctg} \frac{K \sin 2\theta_0}{r_{a_0}^4 + K \cos 2\theta_0}. \tag{4}$$

The particle trajectory will meet the inside surface of the tube at a point whose coordinates are r_{af} and θ_f determined by the system of equations:

$$r_{a_f}^2 = C \sin 2 \left(\theta_f - \alpha \right) \;\;,\;\; r_{a_f}^2 + d_a^2 - 2 r_{a_f} d_a \cos \theta_f = R_a^2. \tag{5}$$

Since $r_{a_0} > d_a - R_a > 1$, from above it follows that $\alpha \approx 0$. At the same time, since d_a is not much larger than R_a, the solution of the system (5) can be approximated to:

$$r_{a_f} \approx d_a - R_a, \;\; \theta_f \approx \frac{1}{2} \arcsin \left[\frac{\left(d_a - R_a \right)^2}{C} \right]. \tag{6}$$

By eliminating the time from Eqs. (1b) and (1c), one obtains an equation which describes the motion along the z-axis for the cases $\theta_0 \neq 0$.

For the case when $\theta_0 = 0$ and θ remains null along the trajectory, it is useful to eliminate the time from Eqs. (1a) and (1c), which gives:

$$\frac{\mathrm{d}\,z_a}{\mathrm{d}\,r_a} = \frac{\overline{v}}{v_m}\frac{2}{R_a^2}\frac{\left[\left(r_a - d_a\right)^2 - R_a^2\right]r_a^5}{K + r_a^2}\,. \tag{7}$$

The solution of this differential equation represents the equation of particle trajectory in the (x, z) plane.

RESULTS OF MATHEMATICAL MODELLING

Figure 2 presents four trajectories obtained with the above model. The four sets of initial conditions are in the $O'x'y'z'$ reference system (Figure 1). The characteristic parameters are $R_a = 6$; $d_a = 8$; $K = 0.8$ and $v_m/\overline{v} = 31.94$.

The isotelic curves are defined as the locus of all points (r_{a0}, θ_0) for which L_{ac} has a constant value. For the analyzed system, characterized by the constructive parameters L, R, d, and a, these curves can be numerically calculated for different values of functional parameters K and $v_m/\overline{v}$. For obtaining the isotelic curves, we used the normalized capture length L_{ac}, defined as:

$$L_{ac} = \frac{v_m}{\overline{v}}z_{af}\,, \tag{8}$$

where z_{af} is the z coordinate of the cross point of the trajectories with the inner tube surface. This variable includes in itself all the parameters specific for the separation cell, both constructive (L, R, d, a, M_s) and operational (b, χ, $\overline{v}$, η, H_0). Finally, it permits direct evaluation of the effect of these parameters upon the separation efficiency.
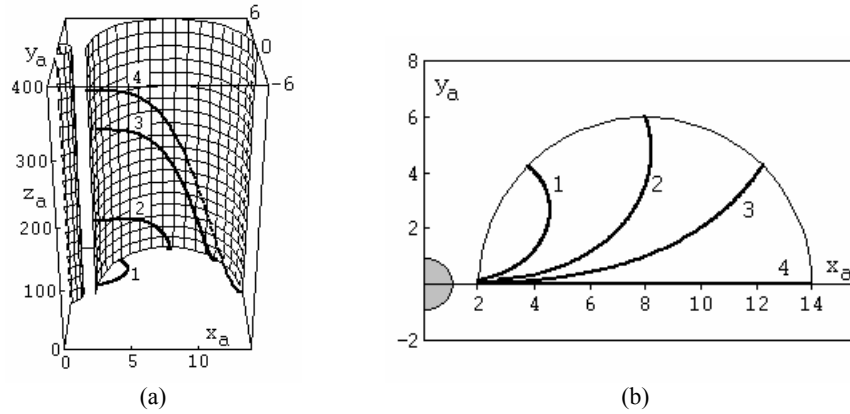
Fig. 2. Trajectories obtained applying the developed model: (a) in 3D space; (b) their projections in the (r,θ) plane. The initial conditions are in the $O'x'y'z'$ reference system (Figure 1): $r_0' = R$, $\theta_0' = 0$ (curve 1); $\theta_0' = \pi/4$ (curve 2); $\theta_0' = \pi/2$ (curve 3); $\theta_0' = 3\pi/4$ (curve 4).
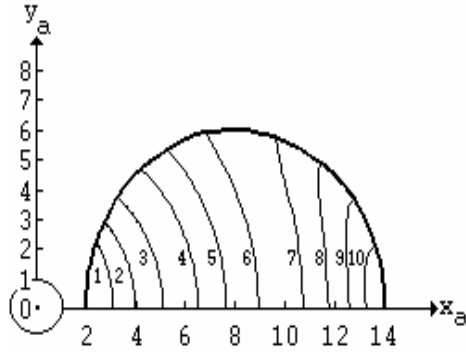
Fig. 3. A group of isotelic curves obtained for:
$K = 0.8$, $R_a = 6$, $d_a = 8$ and $L_{ac} = 10$ (curve 1),
50 (2), 200 (3), 700 (4), 1500 (5), 3000 (6), 6000
(7), 8000 (8), 9500 (9), 10500 (10).
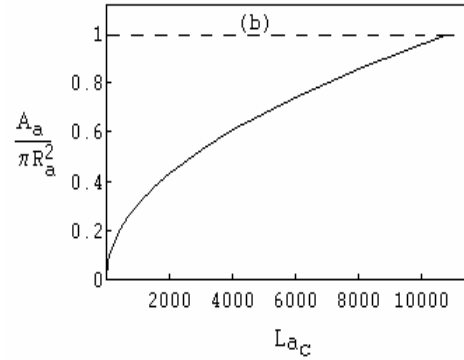
Fig. 4. The ratio between the capture cross-section area and the tube cross-section area *vs.* normalized capture length.

In Figure 3 a group of isotelic curves is presented. All the particles entering the magnetically active space through points situated between an isotelic curve and the tube sector joining the ferromagnetic wire will be captured up to a distance $z_f = L$.

The capture cross-section for a set of parameters represents the area of the tube section limited by the wall joining the ferromagnetic wire and the corresponding isotelic curve. The area of the capture cross-section can be obtained by numerical integration. Figure 4 presents the ratio between the capture cross-section area and the tube cross-section area, *versus* the normalized capture length, for the same characteristic parameters as in Figure 3. One can notice from the very beginning that there is a value of L_{ac} for which this ratio equals unity. Under these circumstances, the capture efficacy in the analyzed separation cell is 100%.

IN VITRO EXPERIMENTAL TESTING

The magnetic separator cell consisted of one glass tube and one stainless steel wire ($M_{s,w} = 1300$ kA/m), positioned at the top of the tube (Figure 5(a)). A relatively homogeneous magnetic field (200 – 440 kA/m) was created by two parallel rectangular NdFeB magnets ($100 \times 100 \times 12$ mm each). The gap between the two magnets is adjustable between 10 mm and 20 mm. The tube-wire setup was sandwiched between the magnets, and high magnetic field gradients were generated by the magnetized wire.

The experimental setup consisted of an AETICS SP-12S PRO universal syringe pump, a magnetic separator cell described above, a receiving container and connecting tubes (Figure 5(b)). The syringe pump drove the sample solution through the separator unit where a fraction of the magnetic spheres was collected against the tube wall and the remaining drained into the receiving container. A SONY DCR HC85E TK-C1380 CCD camera was used to capture the buildup of magnetic microspheres in the separation tube.

(a)

(b)

(c)
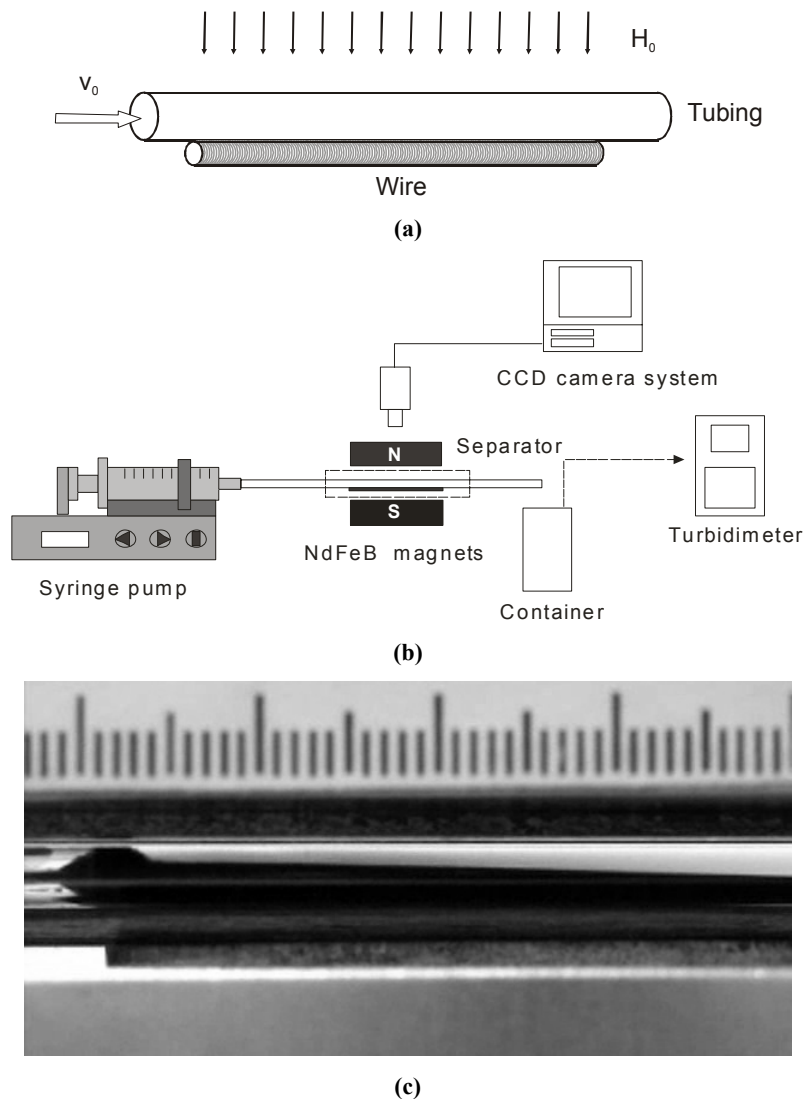
Fig. 5. Experimental setup for *in vitro* flow study: (a) enlarged view of the separator cell; (b) overall depiction; (c) magnetic sphere buildup in the separation system.

Two 0.05 mg/mL solutions were prepared by dispersing in deionized water and in a 44% (v/v) ethylene glycol-water solution, respectively, the weighed dried 1.7 μm magnetic chitosan microspheres containing ~12 % (m/m) magnetite ($M_{s,p}$ = 450 kA/m). The serial dilution of the solution by a factor of 2 and the turbidities of the samples were measured by a 2100P portable turbidimeter.

The capture efficiency (*CE*) of magnetic spheres by the wire-tube system could be calculated using the following formula

$$CE(\%) = \frac{C_{\text{before}} - C_{\text{after}}}{C_{\text{before}}} \times 100 \,, \tag{9}$$

where C_{before} and C_{after} are the concentrations of the sample before and after the magnetic separation, respectively. C_{before} and C_{after} were obtained via concentration–turbidity correlation by the measurement of turbidities of the samples.

At the beginning of each run, the flow system was connected as is shown in Figure 5(b). To study the effect of the mean flow velocity, the variable was varied between 0.15 and 45.0 cm/s. To study the effect of the external magnetic field, the variable was varied between 200 and 440 kA/m. Stainless steel wires with 0.25 mm, 0.5 mm and 1.0 mm in radius and with 3.0 cm, 6.0 cm and 10.0 cm in length were tested, and the capture efficiencies were compared. Also, tubes with different sizes (inner radius of 0.35, 0.75, 1.25 mm, and outer radius 0.5, 0.95, 1.8 mm) were used and the capture efficiencies were compared.

Figure 5(c) shows the buildup of magnetic spheres inside the tube. The conditions were the following: external magnetic field 440 A/m, stainless steel wire with a radius of 0.5 mm and a length of 10 cm, capillary glass tube with 1.25 mm in inner radius and 1.80 mm in outer radius, mean flow velocity 1.0 cm/s. Once magnetic spheres enter the separation area limited by the isotelic curves, they will be subjected to the magnetic force from the magnetized wires and be deflected to the tube walls next to the wire. Moreover, it is easily seen that the distribution of sphere buildup is not homogeneous. We did observe that the magnetic spheres built more at the inlet and less at the middle and outlet of the separation tube.

Figure 6 shows the effect of the applied magnetic field intensity and mean flow velocities on the capture efficiency of the magnetic microspheres from ethylene glycol-water solution. Generally, theoretical results fit experimental results well for H_0= 200 kA/m, 320 kA/m and 440 kA/m against various $\bar{v}$ (Figure 6(a)). However, generally, the theoretical results are smaller than the corresponding experimental values except for low H_0 and/or high $\bar{v}$. This is possibly due to the difference between the magnetization expression in the theoretical model and actual magnetization behavior of those magnetic wires. The results in Figure 6(a) could be further verified by Figure 6(b). For $\bar{v}$ = 5 cm/s and 8 cm/s, the theoretical results are much smaller than the corresponding experimental results at a low magnetic field, which proves the results in Figure 6(a) and is due to the crude magnetization expression in the model. Moreover, the discrepancy between the theoretical and experimental *CE*s was reduced when $\bar{v}$ was increased to 20 cm/s (Figure 6(b)).
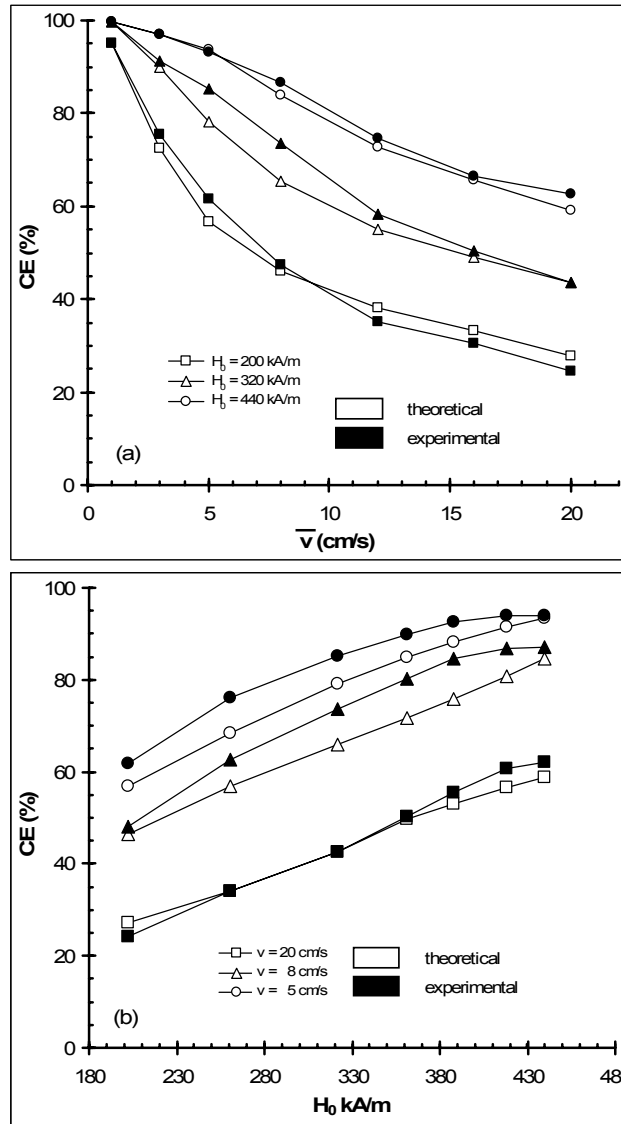
Fig. 6. Effect of the applied magnetic field intensity H_0 and flow velocities $\bar{v}$
on the *CE* of the magnetic microspheres at different flow.

Obviously, the mean flow velocity is a strong factor that affects the *CE* of the system. When H_0 = 440 kA/m, more than 90% experimental *CE* for one flow-through seems feasible provided that $\bar{v}$ < 5 cm/s while only around 60% *CE* is achieved at $\bar{v}$ = 20 cm/s. An increase of the external magnetic field may be helpful to get > 90% *CE* at $\bar{v}$ > 5 cm/s.

CONCLUSIONS

The HGMS magnetic separation cell with the axial configuration analyzed in this paper is adequate for the capture of superparamagnetic nano/micro-spheres in an extracorporeal blood detoxification system. The magnetic capture mechanism discussed here is completely consistent with the properties of the real blood flow, allowing a direct comparison between the theory presented here and the experimental data, using the analytical expressions found for the equations of trajectories.

The theoretical analysis showed that 100% capture efficiency can be reached in the filtering cell, by a proper selection of the geometric and operational parameters. This capture efficiency can be obtained when the capture cross-section area equals the cross-section area of the tube delineating the flow.

The prototype mini magnetic separator device was characterized via a series of *in vitro* experiments using blood mimic fluid (44% ethylene glycol solution. Magnetic separation at various applied magnetic field strengths and various flow rates showed that the device could efficiently separate magnetic spheres from blood mimic fluid at moderate applied magnetic field (< 440 A/m) and relatively high flow rates < 5 cm/s). Around 90% capture efficiency was available at $H_0 = 440$ kA/m and $\bar{v} = 5$ cm/s.

REFERENCES

1. BĂDESCU, V., O. ROTARIU, V. MURARIU, N. REZLESCU, Numerical results and designing aspects concerning the HGMF filtering cells with bound flow field, *Int. J. Multiphase Flow*, 1996, **22**, 797–805.
2. KAMINSKI, M.D., A.J. ROSENGART, Detoxification of blood using injectable magnetic nanospheres: A conceptual technology description, *J. Magn. Magn. Mater.*, 2005, **293**, 398–403.
3. OBERTEUFFER, J.A., Magnetic separation: A review of principles, devices, and applications, *IEEE Trans. Magn.*, 1974, **MAG-10**, 223–238.
4. REZLESCU, N., V. MURARIU, O. ROTARIU, V. BĂDESCU, Capture modeling for an axial high gradient magnetic separation filter with a bounded flow field, *Powder Technol.*, 1995, **83**, 259–264.
5. STAMOPOULOS, D., D. BENAKI, P. BOUZIOTIS, P.N. ZIROGIANNIS, *In vitro* utilization of ferromagnetic nanoparticles in hemodialysis therapy, *Nanotechnology*, 2007, **18**, 495102–495116.
6. STAMOPOULOS, D., Magnetic nanoparticles utilized in hemodialysis for the treatment of hyperhomocysteinemia: The new challenge of nanobiotechnology, *Current Nanoscience*, 2008, **4**, 302–307.
7. WATSON, J.H.P., Magnetic filtration, *J. Appl. Phys.*, 1973, **44**, 4209–4213.